



Feedstock effect on CO₂ gasification of the biomass char generated by fast pyrolysis: a comparative assessment of 40 wood varieties

Shengyuan Guo^{1,2} · Zhimin Lu^{1,2} · Jinzheng Chen^{1,2} · Zhengyan Bao^{1,2} · Jianfeng Cai^{1,2} · Shunchun Yao^{1,2}

Received: 22 December 2022 / Revised: 17 February 2023 / Accepted: 27 February 2023
© The Author(s), under exclusive licence to Springer-Verlag GmbH Germany, part of Springer Nature 2023

Abstract

Char gasification is a feasible technology to recycle CO₂ and utilize biomass energy. However, the impact of different species of biomass on the gasification is still unclear. For the assessment of the feedstock effect on CO₂ gasification, the present work prepared over 40 different wood char samples on a high temperature (around 1523 K) flame reactor, which simulate the rapid heating rates experienced in industrial reactors. Then, the curves of conversion (X) and conversion rate (dX/dt) versus temperature, and the conversion rate versus fractional conversion were derived from the linear non-isothermal thermogravimetric analysis. Three models (volumetric model, grain model, and random pore model) are examined for their goodness of fit between the model and experimental data, and their estimated activation energy. Finally, links between different biomass property parameters and different reactivity indexes were investigated. The results obtained show that different feedstocks result in different gasification reactivities of the resultant chars, with T_{50} and T_{max} varying in a wide range of about 170 K and 200 K. But when conversion is plotted against dimensionless temperature, regardless of the feedstock origin, all the experimental plots can be described by only one curve for $X=0.2-0.95$. We attributed the slightly superior prediction of the RPM to the increased amount of adjustable kinetic parameters, but lower E values were obtained by using RPM. In addition to the potassium content, the cellulose and lignin contents of the feedstock were found to have relatively high correlation with the char reactivity indexes.

Keywords Lignocellulosic biomass · Fast pyrolysis · Feedstock characteristic · Char · CO₂ gasification · Kinetics modeling

1 Introduction

Bioenergy is expected to play an essential role in provision of flexibility in a future energy system dominated by wind and solar power (which often categorized as variable

renewable energy), without the use of fossil fuels. One IEA's 2021 report suggests that the deployment of modern bioenergy needs to increase by 10% per year between 2021 and 2030 to achieve the net zero emissions by 2050 scenario [1]. China's power generation from bioenergy was 163.7 TW·h in 2021, accounting for only 1.9% of the annual power generation [2]. The share is expected to rise to 5% by 2030 [3]. Gasification, among the several thermochemical conversion processes, possesses great potential in the advanced utilization of biomass, producing syngas that can be further upgraded to biogas (methane) directly usable in turbines or vehicles, or from syngas to liquid biofuels (e.g., methanol) to replace diesel and gasoline. Entrained flow gasification (EFG) is the most widely used gasification system because of the high char conversion and low tar yield [4, 5] and can be characterized by the repartition of fast pyrolysis reactions and slow gasification reactions. To realize process optimization as well as feedstock flexibility, the fundamental elements governing the char reactivity during the slow gasification process must be identified, and reliable modeling tools need to be developed to explain the gasification process for multiple biomass feedstock.

Highlights

- The effect of feedstock property on CO₂ gasification has been preliminarily investigated.
- Experimental conditions for char-forming simulate real industrial reactors.
- Different wood species show a similar reaction characteristic.
- A comparison with three models evaluates their feasibility.
- The alkali and alkaline earth metal element and biomass component content have a relatively strong correlation with reactivity indexes.

✉ Zhimin Lu
zhmlu@scut.edu.cn

¹ School of Electric Power, South China University of Technology, Guangzhou 510640, China

² Guangdong Province Key Laboratory of Efficient and Clean Energy Utilization, Guangzhou 510640, China

Literature review [6] showed that the (intrinsic) reactivity for biomass char oxidation or gasification varied by about two to four orders of magnitude. Such a large variability in the reported results is not only caused by the variable properties of the biomass, but also by the different pyrolysis or gasification conditions, making it difficult for comparisons between feedstocks. The differences between wood species have been regarded as relatively small for a long time [6, 7]. In her comprehensive review [6], Di Blasi wrote and we quoted, “contrary to pyrolysis, there is no investigation or evidence available suggesting a relation between the combustion/gasification rate of chars originated from biomass and those from the main biomass components, hemicellulose, cellulose and lignin.” She reviewed the relevant literatures and concluded that inorganic matter was the main factor responsible for the large differences exhibited by chars produced from agricultural residues with respect to wood char for both combustion and gasification. Until now, the majority of the existing work use a couple of biomass feedstocks and then choose either to dope the solid of different inorganic elements or to leach it with aqueous or acid solution [8, 9]. Few authors have increased the raw sample size to over a dozen, and systematically measured the char reaction kinetics and the variation in reactivities between biomass fuels. With the concerns of modification of the biomass structure and the changed dispersion of elements in the char structure by the doping and leaching treatments, Dupont et al. [8] collected 21 wood chip samples from common wood species in France, and correlated the rate of char gasification to the ratio of potassium to silicon in the biomass. Based on a similar idea, they [10] measured the reactivity of 19 biomass species of various types (wood, short rotation forestry, agricultural biomasses, and microalgae) in steam gasification experiments and found a factor of more than 30 between the reactivities of the fastest and the slowest biomass samples. In this work, they highlighted the importance of the ratio $K/(Si + P)$ to predict steam gasification kinetics of biomass chars, because the potassium-rich and silicon- or phosphorus-rich biomasses follow a law of zeroth order and first order, respectively.

Thermogravimetric measurement is the most important tool for studies on solid reactivity. However, the majority of the existing work on the reactivity of biomass char used char generated under low temperature or slow heating pyrolysis conditions (see, for example, the aforementioned Di Blasi's review [6], where she carefully summarized the test results and documented the pyrolysis conditions from relevant literatures due to the great impact of pyrolysis conditions on the char reactivity), which were not representative for the conditions in an entrained flow gasifier. Entrained flow gasification usually operates at high temperatures ($> 1200\text{ }^{\circ}\text{C}$) to achieve a high carbon conversion with rather small particles within a few seconds and produce high-quality syngas

with low or no tar content [11, 12]. Fast heating rates and high temperature pyrolysis experienced in an entrained flow reactor can alter the reactivities of the resultant char in two directions: higher temperature can lead to a decrease, while faster heating rates on the other hand may result in an increase in the char reactivity. The reducing char reactivity with increasing peak temperature and time at temperature is usually described by the term thermal annealing, which is generally attributed to a more ordered, graphitic structure resulting from high-temperature condensations [13]. It is also well-known that faster heating rates during the pyrolysis produce a more reactive char, characterized by a higher total surface area and/or a higher concentration of active sites [6, 13]. Recent study by Septien et al. [14] showed that the faster chemical kinetics of char prepared under high heating rate could be related to both the higher catalytic inorganic content and a more reactive carbonaceous structure.

Char gasification is a complex heterogeneous reaction and the reactivity is affected by many parameters. Many researchers proposed large number of theoretical and semi-empirical kinetics to interpret the evolution of conversion rate. Wang et al. used the volumetric model (VM), the grain model (GM), the random pore model (RPM), and the modified random pore model to describe the kinetics of four herbaceous residue chars and two wooden residue chars [15]. Gupta et al. studied the isothermal gasification kinetics of garden waste chars by VM, GM, and RPM models [16]. The volumetric model, the grain model, and the random pore model are the traditional one-step models with reasonable mechanism assumptions. Substantial research has proven that they could describe the isothermal conversion of biomass char; however, few authors have applied these models to non-isothermal conversion process.

In the current CO_2 gasification study of fast pyrolyzed wood char, the feedstock effect is systematic assessed. Firstly, a large number of different wood samples (45 at first) were collected and processed to make cubic particles with uniform size ($3\text{ mm} \times 3\text{ mm} \times 3\text{ mm}$) and smooth surfaces. Fast pyrolysis of the wood particles at high temperatures ($\sim 1523\text{ K}$) was performed in a hydrogen flame reactor to produce representative chars simulating the realistic conditions encountered in industrial entrained flow reactors. Then, non-isothermal thermogravimetric analyses and kinetic modeling using three representative gas–solid reaction models (the volumetric model, the grain model, and the random pore model) were carried out and the derived reactivity indexes at different conversion stages were correlated with parameters of the feedstock composition, i.e., C/H/N/O elemental content, proximate composition (moisture, volatile matter, fixed carbon and ash), inorganic element contents (K/Na/Mg/Ca/Si/Al), and lignocellulosic composition (lignin, holocellulose, and extractives contents). To the best of our knowledge, similar kinetic study has never been reported in literature.

2 Materials and methods

2.1 Biomass feedstock—stem wood from 45 different wood types

Only stem wood was chosen as our feedstock for some reasons. First of all, woody biomass represents the ideal and the currently most commonly used fuel type in suspension fired reactors, i.e., high-quality biomass fuel without bark and soil containments. Second, woody biomass, as a biomass group, has the minimum ash content and thus, the catalytic effect on the char reactivity can be minimized to emphasize the influences possibly from other biomass properties. Third, the stem wood is easy for batch processing, into regular shape with smooth surfaces, which helps to reduce the uncertainty encountered in the high temperature flame reactor experiments [17, 18]. Finally, its property is less influenced by the growth processes and fertilizer/pesticide usage, as some studies indicated that wood species grown in different regions showed small differences of elemental composition [19].

Stem wood samples from 45 wood varieties were collected. Thirty of them came from a wood farm in Huizhou, Southern China (E114°11', N23°66'), in the form of a whole debarked trunk (diameter of about 0.25 m, length of about 2.5 m). The other 15 wood samples are supplied by different suppliers in the timber market, in the form of 3 * 3 mm cubic rods. These 45 wood samples were then cut into 3 * 3 * 3 mm wood cubes, with a length variation of ≤ 0.3 mm. Proximate analysis, ultimate analysis, biomass components analysis (by the Van Soest method [20]), and ash composition analysis (by inductively couple plasma method) were carried out, and the results are shown in Fig. S1, Fig. S2, Fig. S3, Fig. S4, Table S4, and Table S5.

2.2 Char preparation from fast pyrolysis

The cubic wood particle was inserted into a single particle hydrogen flame reactor one by one, to produce fast pyrolyzed char. The flame temperature (ca.1523 K) and the estimated heating rate (ca.200 K·s⁻¹) inside the single particle reactor (i.e., SPR) were close to the realistic conditions in a large pulverized wood fired reactor [21]. A detailed description of the combustor and the experimental procedures can be found elsewhere [17, 21, 22]. The fast pyrolysis processes were recorded by high-speed cinematography. Post processing of the videos showed that the char particles were removed from the center of the SPR right after the extinction of the volatile flame in less than 0.2 s and were retracted back to the water-cooling and nitrogen-filling chamber in less than 0.4 s after the particle flame extinction. Five char particles for each wood variety were collected for later kinetic experiments. No further analyses of the char samples have been carried out so far,

because of the difficulty to produce enough quantity of char from the single particle reactor, where just a couple of milligrams is obtained in each experiment.

2.3 Char gasification by non-isothermal TGA approach

The SPR-generated char particles were grounded carefully in a mortar and pestle. Char gasification was performed in a thermogravimetric analyzer (TGA, Netzsch STA 449F1 Jupiter). During the TGA analysis, firstly pure CO₂ was purged into the machine to remove residual air and then, ~1.0 mg of the char powder was heated from 110 °C (before which was the drying, the stabilization stage) to 1000 °C at a heating rate of 10 °C/min under an atmosphere of pure CO₂. Sufficient CO₂ through the char is requiring eliminating the effect of external diffusion on the gasification rate, and a gas flow of 80 mL/min was recommended in the literature [23]. In this research, a continuous CO₂ flow of 100 mL/min was selected. The moderate heating rate, small sample mass, and sufficient reactant flow guarantee the absence of mass transfer limitations and self-heating effects [24, 25]. Duplicate tests showed a good reproducibility as standard errors of weight loss were within 0.5% at any temperature. Hence, only the averaged thermogravimetric curve is reported.

2.4 Gasification kinetic models

Based on the measurement of weight loss versus time, the gasification conversion (X) was calculated using the following formula:

$$X = \frac{m_0 - m_t}{m_0 - m_\infty} \quad (1)$$

where m_0 represents the initial mass; m_t is the instantaneous mass of the char at time t ; and m_∞ is the mass of gasification residue in char after complete reaction.

The average reactivity r_{integ} was defined between two stages of conversion X_1 and X_2 by Eq. (2):

$$r_{\text{integ}} = \frac{\int_{t_{X_1}}^{t_{X_2}} \frac{r(t)dt}{1-X(t)}}{t_{X_2} - t_{X_1}} \quad (2)$$

Note that there is no standardized interval of the conversion X . In the literature, Sorensen et al. [26] worked on an interval of conversion ranging from 0.2 to 0.8, and Tagutchou et al. [27] made the calculation with an X interval ranging from 0.15 to 0.9. In previous studies, researchers always chose intermediate conversion ranges with low uncertainty for standardized calculation. This research would choose the interval of X on the basis of experimental results.

A general kinetic expression for the overall reaction rate in gas–solid reactions is written as the following equation [28]:

$$\frac{dX}{dt} = k(T)f(X) \quad (3)$$

where k is the apparent gasification reaction rate constant, which is determined by temperature (T) and can be expressed by the Arrhenius equation as Eq. (5) [29]:

$$k = k_0 e^{-E/RT} \quad (4)$$

where k_0 , E , and R are the pre-exponential factor, activation energy, and universal gas constant, respectively. Structural or surface function $f(X)$ refers to the reactive surface related to the reaction mechanism. In this study, three most commonly used nth-order kinetic models, namely, the volumetric model (VM), the grain model (GM), and the random pore model (RPM), were applied to describe the gasification kinetic of the fast pyrolyzed wood char.

The VM model is the simplest model, which assumes the gasifying agents react with char particle at uniformly distributed active sites [30]. Any possible structural changes of the solid sample during the reaction are neglected. The GM model, also known as the unreacted core model [31], assumes that a porous medium is comprised of a group of uniform, nonporous, and spherical grains, and the reaction first occurs at the external surface of grains before moving progressively within. The RPM model, which simultaneously considers the effects of pore growth in the initial stages and the destruction of pores due to the coalescence of adjacent pores during the later course of gasification, normally gives improved prediction and shows a maximum of reaction rate at the conversion lower than 0.393 [32]. These three models give different formulations of the term $f(X)$. Their basic equations are listed as follows:

(1) VM model

$$\frac{dX}{dt} = k_{VM}(1 - X) \quad (5)$$

(2) GM model

$$\frac{dX}{dt} = k_{GM}(1 - X)^{2/3} \quad (6)$$

(3) RPM model

$$\frac{dX}{dt} = k_{RPM}(1 - X)\sqrt{1 - \psi \ln(1 - X)} \quad (7)$$

where ψ is a parameter related to the pore structure of the unreacted sample ($X = 0$).

The temperature-programmed reaction (TPR) [33] technique involves heating the samples at a constant rate, a . The temperature, T , is related to time, t , by [30]:

$$T = T_0 + at \quad (8)$$

Under the linear non-isothermal conditions, the above three kinetic equations at isothermal condition can be transformed into the following Eqs. (9), (10), and (11) [34].

$$\text{VM} : X = 1 - \exp\left(-\frac{RT^2}{aE_a}k_0e^{-\frac{E_a}{RT}}\right) \quad (9)$$

$$\text{GM} : X = 1 - \left(1 - \frac{RT^2}{3aE_a}k_0e^{-\frac{E_a}{RT}}\right)^3 \quad (10)$$

$$\text{RPM} : X = 1 - \exp\left\{-\frac{RT^2}{aE_a}k_0e^{-\frac{E_a}{RT}}\left[1 + \frac{\psi}{4}\left(\frac{RT^2}{aE_a}\right)k_0e^{-\frac{E_a}{RT}}\right]\right\} \quad (11)$$

The least square method was used between experimental data and kinetics models to yield the ratio of the activation energy to the ideal gas law (E_a/R) and pre-exponential factor (k_0). This method calculates the suitable values of E_a and k_0 based on the least error between experimental and model data. The advantage of this method is that the values are relatively precise for the whole reaction. The numerical procedure is implemented in the software Python.

To compare the accuracy of kinetic models, the average values of deviation (DEV) between the experimental and simulated conversions and reaction rates were calculated according to Eqs. (12) and (13) [30]:

$$\text{DEV}(X)(\%) = 100 \times \frac{\left(\sum_{i=1}^N (X_{\text{cal},i} - X_{\text{exp},i})^2 / N\right)^{1/2}}{\max X_{\text{exp}}} \quad (12)$$

$$\text{DEV}\left(\frac{dX}{dt}\right)(\%) = 100 \times \frac{\left(\sum_{i=1}^N \left(\left(\frac{dX}{dt}\right)_{\text{cal},i} - \left(\frac{dX}{dt}\right)_{\text{exp},i}\right)^2 / N\right)^{1/2}}{\max\left(\frac{dX}{dt}\right)_{\text{exp}}} \quad (13)$$

where N is the number of test value during the reaction, $\max X_{\text{exp}}$ represents the maximum value of the experimental curve, $X_{\text{exp},i}$ and $X_{\text{cal},i}$ are the experimentally obtained and model calculated values for X , respectively, and $\left(\frac{dX}{dt}\right)_{\text{exp},i}$ and $\left(\frac{dX}{dt}\right)_{\text{cal},i}$ represent the experimental conversion rate and model fitted conversion rate.

3 Results and discussion

3.1 Non-isothermal gasification curves

TG and DTG curves of the linear non-isothermal gasification of the fast pyrolyzed chars prepared from 45 different wood varieties were drawn. Five samples display a strange and unexpected second weight loss behavior in the main char conversion regime, clearly implying the existence of two char fractions with different reactivities, probably attributed to the different chemical natures of the precursors. This two-stage feature of char oxidation has seldomly been reported in the literature. Indeed, it has only been reported for dry distiller's grains with solubles (DDGS) [35, 36], and for banana peel [37]. Carmen Branca and Di Blasi suggested that single well-defined reaction zone was generally observed for lignocellulosic chars, while the two distinct zones especially the second one evolving at much higher temperatures had a peculiar behavior and only had been observed for DDGS. Further tests and more analyses are needed to provide explanations for these behaviors, which is beyond the scope of the present study.

In the following text, only the results from the other 40 wood varieties were shown and discussed. Their TG and DTG curves are shown in Fig. 1. Similar qualitative trends are observed in all cases. In Fig. 1a, the conversion starts slowly from a very low temperature right after the drying stage until reaching the conversion $X = 0.15$ – 0.2 . From then on, over the conversion period from 0.2 to 0.95 , there appears a steep spike, followed by a flatten part over the remaining conversion range of 0.95 – 1.0 ; different feedstocks result in different gasification reactivities of the resultant chars, with T_{50} varying in a wide range between 1018 and 1187 K, an interval of about 170 K. But from the qualitative point of view, all the curves present the same shape.

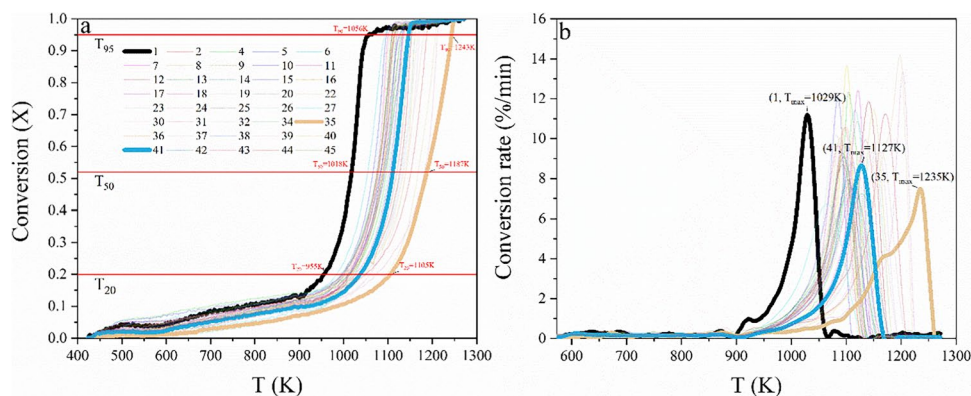
On the other hand, all DTG curves (Fig. 1b) consist of a more or less pronounced shoulder, followed by the attainment of a peak rate. The shoulder and peak in the

DTG curves fit the description of the char devolatilization stage and oxidation stage introduced by Di Blasi [24, 38] very well, except that in our case the CO_2 gasification instead of O_2 oxidation is the cause of the solid conversion and weight loss. Although it is more or less feedstock dependent, it is clearly shown in Fig. 1b that the temperature has a great influence on CO_2 gasification kinetics of the fast pyrolysis char—the reaction rate is almost negligible below 900 K, and strongly increases above 950 K. Beyond the well-defined peak, the reaction rate plummets in a very similar slope for all samples. The variations in DTG_{max} , the maximum conversion rate, are relatively small (5.74 – $14.98\%/ \text{min}$), while the corresponding temperature to obtain the maximum conversion rate, T_{max} , shows a great spread from 1029 to 1235 K (an interval of about 200 K). The final stage corresponds to a flat zone as it is associated with the very last $\sim 5\%$ of char slowly oxidized at higher temperatures (starts from around 1070 to 1260 K dependent on char origins) in the so-called ash cooking zone [25].

The shoulder or extra peak (if any) represents at least one reaction step. Branca et al. [39] suggested that the shoulder in the thermogravimetric curves of char can be attributed to the further decomposition of cellulose and lignin macro-components. Considering the char in the present study was made in a dynamic flame environment (Sect. 2.2), without enough soaking time under high temperature environment, it seems reasonable that the decomposition of some macro-components remains incomplete and further decomposition of heteroaromatic structures and formation of polyaromatic structures are expected to occur, particularly in the inner layer of the relatively large particle. Therefore, only the conversion range of 20 – 95% would be considered and analyzed in the following.

In consideration of the remarkable similarities in the trends of the curves of char conversion versus temperature observed in Fig. 1a, the curves were replotted against the normalized temperature, T/T_{50} , where T_{50} is the

Fig. 1 Non-isothermal conversion curves (a) and DTG (b) of fast pyrolyzed char samples prepared from 40 different wood varieties. TGA condition: from 383 to 1273 K at a heating rate of 10 K/min in CO_2 atmosphere



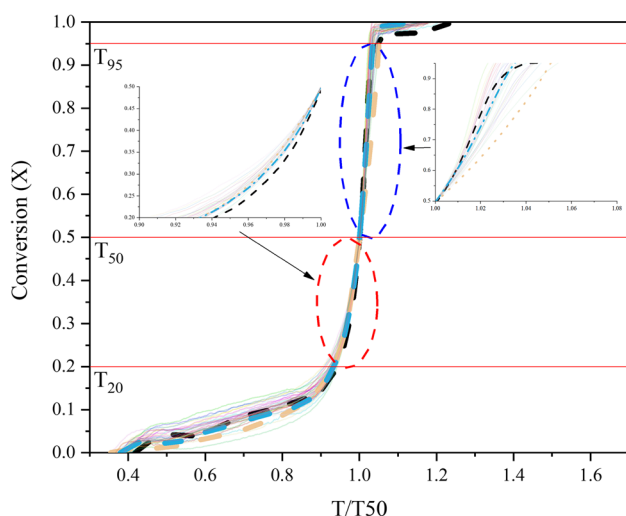


Fig. 2 Conversion curves versus the normalized temperature, T/T_{50} , with zoom-in views of the conversion regions of 0.2–0.5 and 0.5–0.95. Legends are the same as shown in Fig. 1

temperature to obtain 50% conversion (Fig. 2). It is clearly shown that the origins of the fast pyrolysis char do not affect the qualitative features of the TGA conversion curves. Taking only the conversion range of 20–95% for consideration, at the conversion of 50%, the normalized temperature equals one for sure. But at the conversion of 20% and 95%, the normalized temperature only varies in a very small range of around 0.9–0.94 and 1.02–1.05, respectively, suggesting that the normalization works perfectly in the aforementioned range. The visual observation of the measured curves does not allow a clear demarcation between the char devolatilization and the char gasification. In the present study, we arbitrarily determined that the main char gasification stage ranged from $X=20$ to $X=95\%$.

3.2 Comparison of reaction rates

The conversion stage average reaction rate r_{integ} between two stages of conversion was calculated as previously done by Dupont et al. [8] and is shown in Table S6. The values obtained between conversions of 20–95%, representing the full range of char gasification for 40 samples originated from different wood varieties, are shown in Fig. 3a. The feedstock-mean value of r_{integ} was of about 0.25%/min, with a variation of a factor of 2.7 between the minimum and maximum among the samples. The minimum and maximum values of reaction rates were attained by wood 22 and wood 30, respectively, with the average reaction rate of 0.19%/min and 0.35%/min. In this research, wood 1 and 35 were chosen to analyze more details since wood 1 was the first to finish the conversion stage and 35 was the last to complete the reaction. Wood 41 was also selected for further discussion,

whose r_{integ} was of about 0.25%/min (equals to the feedstock-mean r_{integ}), as a representative feedstock. It is significant to note that the three samples of wood 1, 35, and 41 have some characteristics that are the lowest, highest, and closest to average of all the samples. This results in the fixed carbon and char yield to have the similar order. Furthermore, the range of potassium content and magnesium content for three samples accounted for 63.4% and 68.5% of all samples respectively. Their ranking of potassium content and magnesium content is the same, wood 41 > wood 1 > wood 35. The sodium and calcium contents of the three samples are very close. These three feedstocks were also highlighted in Fig. 1 and Fig. 2.

The origins or the growth processes of the wood samples did not seem to have any systematic influence on char reactivity, since in Fig. 3 the white column representing those chars from merchantable wood and the filled column representing those chars from wood samples collected in one wood farm are evenly distributed. Also, the difference of reaction rate did not appear to be correlated with the species themselves. For instance, the two samples of pinewood: wood 11 and wood 14, had different reaction rates (0.22%/min versus 0.29%/min). These two pinewood samples have fairly similar Na, Ca, and Mg contents, but their K content differed by a factor of 2.4 (264 mg/kg versus 628 mg/kg). Again, their reactivity difference seems to be explainable by their variances in catalytic element contents.

Average reaction rates on the whole range of char conversion (20–95%) vary only modestly among the 40 woody samples. Following previous work [8], the average reaction rate r_{integ} was calculated in narrower ranges of conversion and its variations were analyzed to see whether these reactivity differences were sensible along the whole range of conversion or specifically in a specific narrow range of conversion. This may help to better understand the mechanisms, particularly the role of the catalytic elements played on the conversion rate. Recent investigations [40–43] have shown that the average reaction rates of biomass chars vary with the char conversion ratios. Most of them agreed that the catalytic or inhibiting effects exerted by the inorganic elements were the major parameter influencing reactivity at high conversion ratios (e.g., $X > 60\%$).

Figure 3b to 3e present the r_{integ} of the 40 char samples for specific conversion ranges of 20–40%, 40–60%, 60–80%, and 80–95%, respectively. The corresponding feedstock-mean values are of about 0.047%/min, 0.16%/min, 0.51%/min, and 1.51%/min, respectively, becoming progressively higher. Additionally, the variation factors (ratio of the maximum and minimum values) were of about 1.8, 1.8, 3.3, and 4.6, respectively, for the four conversion stages, indicating the reactivity difference between different feedstock was enlarged with the progress of reaction. The results confirm that with progressively release of the C, H, and N during

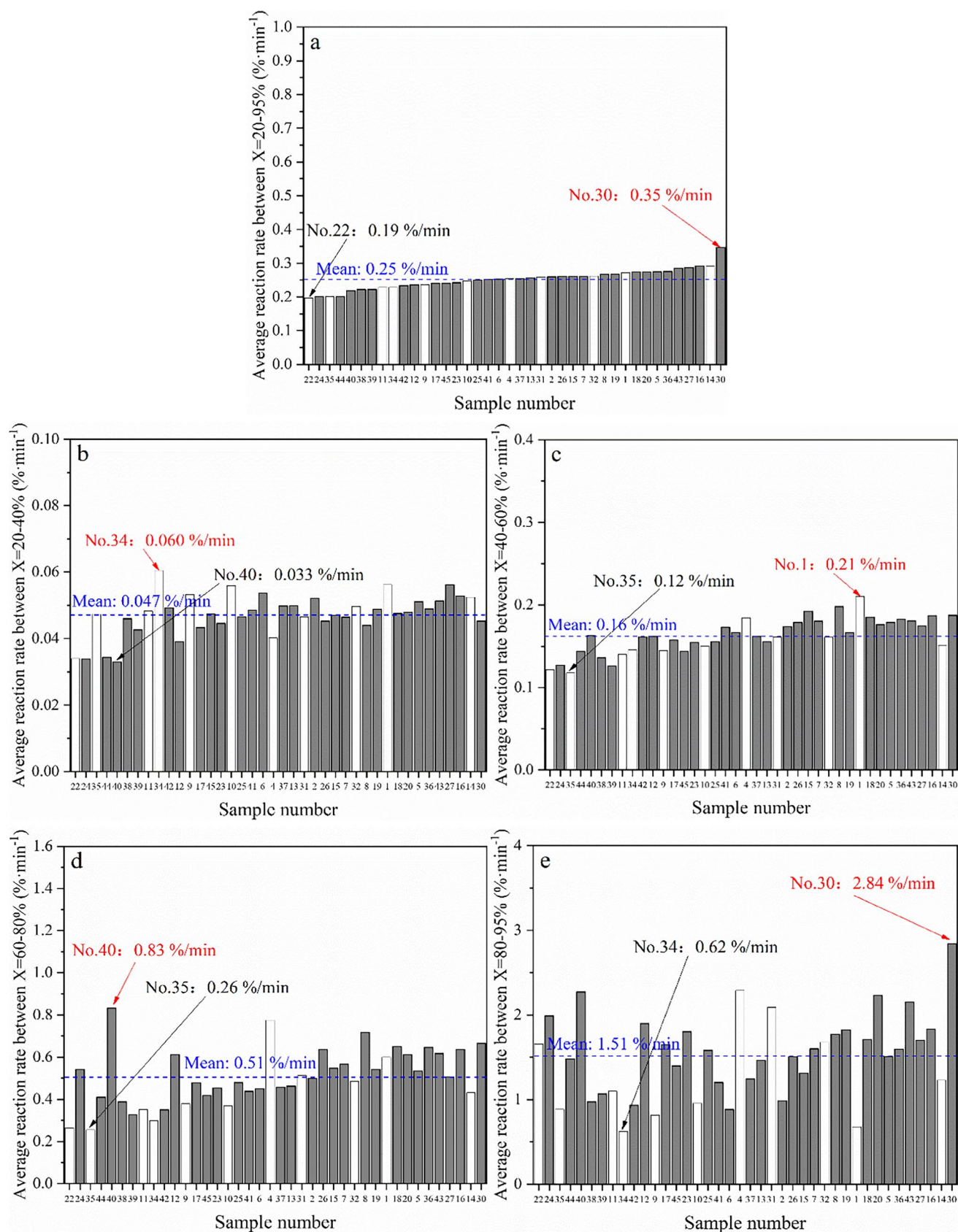


Fig. 3 Average reaction rate of 40 char samples at different conversion ranges: **a** 20–95%; **b** 20–40%; **c** 40–60%; **d** 60–80%; **e** 80–95% (white column: those from merchantable wood, filled column: those from wood samples collected in one wood farm)

char gasification, the inorganic material is majorly retained within the residue char, and therefore, the amount of alkali catalyst per unit available char surface area (or unit mass of char) increases with progressing gasification, which can explain the gasification acceleration and also the enlarged reactivity variation observed here. This observation that the average reaction rate tended to increase with conversion is in accordance with the isothermal steam gasification research by Dupont et al. [8], only their average reaction rates are much higher, which can be explained by the more active gasifying agent (steam) and higher overall reaction temperature (800 °C) used in their TGA experiment.

3.3 Kinetic analysis

3.3.1 Performance of VM, GM, and RPM models

Regarding the variation of the char reactivity in the CO₂ gasification experiment, three reactivity models (VM, GM, and RPM) are examined in the present work using the linear non-isothermal TGA experimental data for 40 fast pyrolyzed wood chars. It is worth noting that all chars exhibited the similar fitting trends; however, for practical reasons, just three chars with the fastest (wood 1), the slowest (wood 35), and the average (wood 41) reactivity are shown in the figures.

Figure 4a–4c show the fitting of the conversion and conversion rate (DTG) curves from three selected wood feedstock to the volumetric (Eq. (9)), grain (Eq. (10)), and random pore (Eq. (11)) reaction models. On the whole, performances of these three models are pretty similar: they all underpredicted the conversion below $X=0.3$ and above $X=0.7$ (for RPM the underprediction is milder, particularly between $X=0.7$ and 0.8), independent of the feedstock effect; the predicted profiles of the conversion rate are all border and shorter than the measured ones—none of the three models captures the sharp peak exhibited by the experimental curve of conversion rate; when plotted against conversion, the VM, GM, and RPM again fail to describe the experimental rate maximum beyond $X=0.7$. The acceleration in the earlier stage can be explained by the increasing temperature adopted in the non-isothermal approach, and the deceleration occurred later in the conversion process is caused by the reduction in residue mass to be reacted.

Table 1 enables a quantitative comparison, by listing the DEV (X) and DEV (dX/dt) for three representative wood varieties predicted by the three models. As shown, the RPM has a slightly better fitting performance consistently than VM and GM. In the extended research, shown in the supplemental material (Table S2), RPM outperforms for the majority wood types (wood 5, 36, and 37 were exceptional). The second observation is the DEV (X) value is much smaller than the DEV (dX/dt) value, which is consistent with the literatures [30, 31]. Lastly, all three models performed better

for wood 1 than the other two wood samples, but only to a modest extent. It seems reasonable considering the great similarities among different feedstocks (Fig. 2) and the systematic deviation below $X=0.3$ and above $X=0.7$ between the experimental and theoretical conversion data (Fig. 4).

Several authors [15, 44–47] have assessed the performance of different models, including VM, GM, and RPM, to describe the gasification curve of char under CO₂ atmosphere. Mostly, they concluded that only the RPM accurately (acceptably) predicted the conversion of different biomass chars. A closer examination of the prediction errors or model deviations would suggest that the RPM predictions may have the smallest deviations from the experimental data among the three models; however, its superiority over the other models is often only modest [44, 46], and sometimes the deviation is still significant [47].

3.3.2 Estimation kinetic coefficients

Complete data of the fitted CO₂ gasification kinetic parameters of the 40 wood chars estimated by the RPM, VM, and GM models, along with the regression coefficients (R^2) and average value of deviation (DEV), are supplied in the Tables S1 and S2 as supplemental material. The accuracy of model prediction is usually assessed based on either the regression coefficients (R^2) or some sort of deviation index (for example, the average value of deviation used in the present study). It is noted that the R^2 are significantly higher, and the DEV values are significantly lower for model predicted conversions than for the predicted conversion rates.

As indicated in Table S1, RPM is superior to the other two models, only when comparing the feedstock-average regression coefficient (0.990 for the former versus 0.989 and 0.986 for the latter two), which confirmed the great similarity in their prediction accuracy. The minimum determination coefficient of the model fitting to the experimental results is 0.935 for RPM, 0.938 for VM, and 0.977 for GM. Such a high value of determination coefficient justifies the correctness of the model fitting and the estimated kinetic parameters [29, 48, 49].

Figure 5 shows a box plot created by the software Origin, indicating the statistic of the activation energies (E) and the pre-exponential factors (A) for CO₂ gasification of 40 wood char samples. The feedstock-average E is 143.2, 195, and 173.8 kJ/mol for RPM, VM, and GM respectively, and the maximum and minimum values are 111.1 and 170.6, 151 and 234, and 137.1 and 206.4 respectively. The values obtained in this study are clearly dependent on the kinetic models used. The trend that lower E values were obtained by using RPM coincides with the literature [45][45]. From the above analysis on the model prediction accuracy, it cannot be concluded which value is more appropriate for describing fast pyrolyzed char gasification in CO₂ atmosphere.

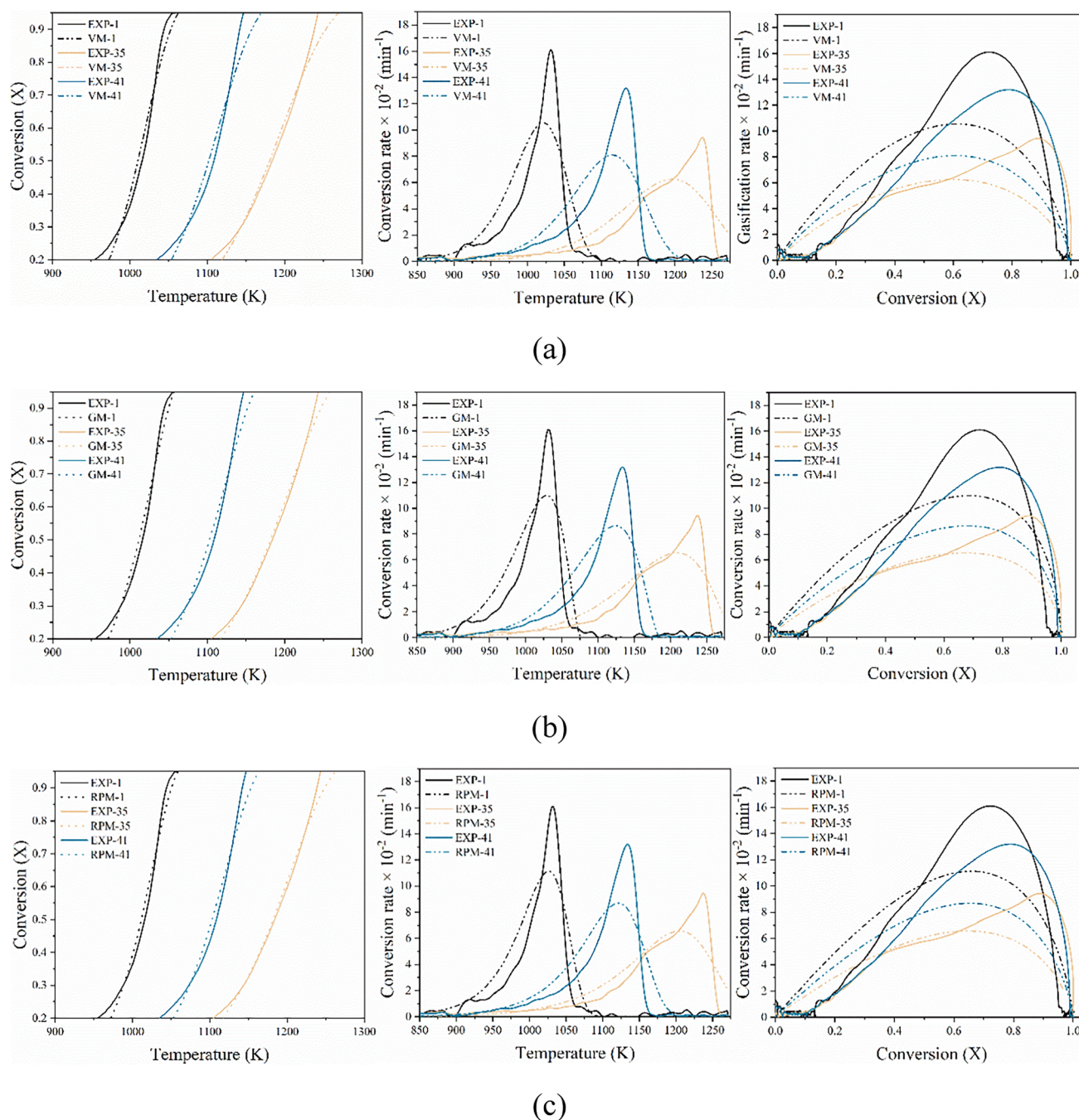


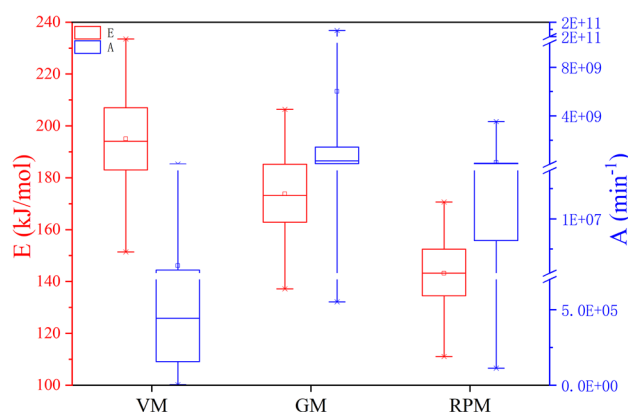
Fig. 4 Experimental and predicted curves of conversion (left), conversion rate (middle) with TGA temperature as function, and conversion rate with conversion as function (right) for three selected chars: **a** VM model; **b** GM model; **c** RPM model

A wide range of activation energies has been reported in the literature for CO₂ gasification of biomass chars. In Di Blasi's review [6], the reported activation energies vary between 88 and 250 kJ/mol, with a large part of the values around 200–250 kJ/mol. In a more recent review on the CO₂ char gasification from 2014 to 2020 [50], a similar range (from 100 to 247 kJ/mol) for the biomass char only can be extracted from the summary table.

The predicted activation energies by the three models in this study all fall within the scope of the literature reported values, although the values obtained by the VM are closer to the normal range indicated by Di Blasi (200–250 kJ/mol). The wide dispersion of the E values reported from different studies might be caused by the influence of many different variables, such as biomass properties, pyrolysis, and gasification conditions

Table 1 Estimated kinetic parameters, adjustable parameters of the RPM, VM, and GM models for three selected samples

| Sample number | 1 | 35 | 41 |
|----------------------------|----------|----------|----------|
| VM | | | |
| E (kJ/mol) | 232.1 | 183.3 | 209.6 |
| k_0 (min ⁻¹) | 1.88E+11 | 1.42E+07 | 1.24E+09 |
| DEV (X) (%) | 6.74 | 4.90 | 6.00 |
| DEV (d X /d t) (%) | 10.2 | 10.38 | 10.24 |
| GM | | | |
| E (kJ/mol) | 201.0 | 159.7 | 186.3 |
| k_0 (min ⁻¹) | 3.53E+09 | 9.74E+05 | 7.59E+07 |
| DEV (X) (%) | 6.76 | 4.43 | 6.57 |
| DEV (d X /d t) (%) | 10.61 | 9.39 | 10.34 |
| RPM | | | |
| E (kJ/mol) | 168.5 | 132.9 | 153.7 |
| k_0 (min ⁻¹) | 4.46E+07 | 3.90E+04 | 1.27E+06 |
| ψ | 4.96 | 4.58 | 5.11 |
| DEV (X) (%) | 6.38 | 4.24 | 5.55 |
| DEV (d X /d t) (%) | 10.01 | 9.33 | 9.79 |

**Fig. 5** Box plot indicating the maximum, minimum, median, average values, and the interquartile range of the E and A fitted by RPM, VM, and GM models for 40 wood char samples

(temperature range and temperature-programmed used, gasifying agent concentration) or type of reactor used. Even the kinetical model and the analytical method used [50] can play an important role in the determination of the kinetics parameters. The present work prepared the char in identical experimental setup and deduced the kinetic parameters under the same experimental and model fitting condition for different wood types; a wide range of the kinetic parameters indicated by Fig. 5 would suggest that the intrinsic biomass characteristics influenced their reactive behavior.

3.3.3 Further discussion

Note that the main differences between the three models lie in (i) the assumptions on the particle structure and hence reactive site locations when taking a microscopic view [51]. The chemical reaction is assumed to taking place either simultaneously at all points within the particle (the volumetric model) or at the outer surface only (the grain model, also known as the shrinking core model). RPM furtherly considers the evolution of char structure and hence the reactive site concentration as gasification proceeds; (ii) the capacity to describe the experimental data with a maximum value in the reactivity-conversion curve when using a macroscopic modeling approach. The former two models are incapable while the RPM can describe a maximum in reaction rate.

A survey of literature revealed some unanswered questions and limitations of the commonly used random pore model:

(i) Gomez et al. [52] questioned the existence of the maximum reaction rate. He provided quite convincing experimental evidences to prove that the maximum reaction rate during isothermal gasification experiment is just a consequence of switching the inert gas for the gasifying agent [52, 53], and not due to changes in the char surface during gasification, as suggested by the RPM. If the gas switching and thus the gas dispersion effects can be avoided by adjusting the experimental procedure, the VM and the ICM (integrated core model) fit better to the experimental results than the RPM [52, 54]. Observations obtained by the present study on the RPM's superiority over the other two models may be just a consequence of an increase in the number of fitting parameters. In view of the faulty experimental procedure of the isothermal approach, the present study may be a solution for switching gas problem and for verifying the reasonableness of RPM assumptions.

(ii) The popularity of the RPM is mainly due to its non-linear dependence on char surface, taking into account the effects of pore growth and coalescence during reaction and enabling the prediction of a maximum reactivity as being observed in some experiments. However, the original RPM fails to describe the reactivity profiles of biomass chars or alkali metals catalyzed carbons, in which the reactivity increases with increasing conversion or exists a maximum in high conversion range ($X > 0.393$) [55–57]. Theoretically speaking, the change in intrinsic reactivity (free from any mass transfer limitation) can be associated to the change in any other influential factors of the char reactivity. For example, the content, dispersion, sintering, or inhibition of the catalyst-species all cannot be assumed to be constant properties during the course of reaction and should play important roles, especially for

biomass char conversion. As shown in Fig. 4, the RPM fails describing our experimental rate maximum of the wood char, which appeared at high conversion (beyond 0.7). More complex model (for example, the modified random pore model [56], or and the extended random pore model [55, 58], both seem promising to quantify and interpret catalyst effects in biomass char gasification) should be explored for better description of the experimental data, which will be our work in the next stage.

(iii) Literature [51, 59] has found that the RPM may respectively overestimate and underestimate the conversion rate in the intermediate stage and in the later stage, as also indicated by the Fig. 4c in the present study.

3.4 Correlations between gasification reactivity and biomass properties

The term reactivity refers to a property of the solid fuel as its capacity for chemical reaction [16]. In this context, various reactivity indexes can be used. Scatter diagram and Pearson's product moment correlation were used to determine the relationship between different fuel property parameters and gasification reactivity indexes. The parameters describing the fuel properties include proximate analysis (moisture, volatile matter, fixed carbon and ash content), ultimate analysis (C/H/N/O content), inorganic compositional analysis (K/Na/Ca/Mg/Si/Al content), and lignocellulosic compositional analysis (hemicellulose, cellulose, and lignin content). The used reactivity indexes are five average reaction rates (as shown in Fig. 3, namely, R20-40, R40-60, R60-80, R80-95, and R20-95) and four more frequently used indexes, i.e., R50, T50, R_{\max} , and T_{\max} , representing the conversion rate and the temperature when reaching 50% conversion, the maximum conversion rate, and the temperature to obtain it. The former five report the average reaction rate over a conversion range, and the latter four are defined at a specific value of conversion. Moreover, the former four might be independent to each other, while for the latter four, the higher conversion rate (R50 or R_{\max}) means higher reactivity and the higher T50 and T_{\max} are related to lower reactivity.

The results of the correlational analysis are illustrated in the supplemental material as a correlation matrix (Table S3), with the fuel property parameters and reactivity indexes listed as row headers and column headers, respectively. A glance through the cell figures representing the correlation coefficients reveals a pretty low correlation strength. Figure 6 presents the correlation between potassium content and the five average reaction rates. The strongest correlation exists between the potassium content of the feedstock and the R60-80 (average reaction rate at conversion range of 60–80%), with a positive correlation coefficient of 0.56. Note that K content also has a pretty strong correlation with

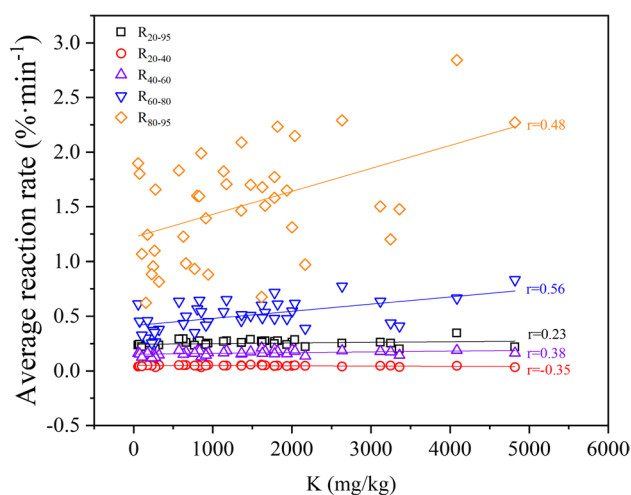


Fig. 6 Correlation between potassium content in feedstock and average reaction rate at different conversion ranges

R80-95 and R_{\max} (correlation coefficient of 0.48 and 0.44, respectively). Interestingly, there are apparent correlations between the cellulose and lignin content with the reactivity indexes pairs of R50 and T50, and also R_{\max} and T_{\max} . Cellulose content correlates best with R50 with a correlation coefficient of 0.48, while lignin content's correlation coefficients with T50 and T_{\max} are both higher than 0.46. Worthy of mention also is the consistency of these two lignocellulosic composition parameters, i.e., cellulose content is positively correlated with both the conversion rates (R50 and R_{\max}) and negatively correlated with both the temperature reactivity indexes (T50 and T_{\max}), while lignin content is on the opposite. From this perspective, silicon, the well-known element with an inhibitory effect on the conversion rate, exhibits a consistently negative (although very low) correlation with all the conversion rate indexes and positive correlation with the temperature reactivity indexes. All the other fuel property parameters exhibited little if any correlation with the reactivity indexes. Sodium might be an exception, but its content only correlates with R40-60 ($r=0.42$) and correlates poorly with other indexes. Besides, the Na contents in the feedstocks are very low (a range of 50.0–124.0 mg/kg and the average value is 75.0 mg/kg), compared to other elements.

Considering the large sample size (40 feedstock in the present study, such a large number of woody biomasses as experimental subjects is unknown in literature to the authors), we therefore conclude that the reason for the relatively low dependence of the gasification reactivity indexes on the potassium content or any other ash compositions is because of the very low variation in the content of our tested feedstock. Dupont et al. [8] obtained a comparatively high linear correlation ($R^2=0.77$) of the

corrective kinetic parameter a_i from a modified grain model versus the ratio K/Si, with 21 different wood chips as feedstock. Their feedstock has a comparatively larger variation in the content of inorganic composition, with ash, K, and Si content spreading in a range of 0.5–4.3%, 112–2019 mg/kg, and 85–3619 mg/kg, respectively. They later studied 19 biomass feedstocks [10], which belong to 4 classes: wood (5 samples), SRF/SRC (short rotation forestry/coppice, 4 samples), agricultural residue (8 samples), and microalgae (2 samples), and divided them into 3 families according to their ratio K/(P + Si). When the ratio is larger than 1, the kinetic parameter k_1 can be satisfactorily correlated ($R^2 = 0.72$) to the potassium concentration in the feedstock. Extracting the data from their paper, we can find a significantly large variation in the content of inorganic composition even only in the so-called family 1, with ash, K, and Si content ranging from 0.4 to 14.7%, from 0.021 to 2.57%, and from 0 to 10.17%, respectively. For comparison, in the present study the content variations of ash, K, and Si content are significantly minor: ranging from 0.63 to 1.16%, from 0 to 0.48%, and from 0 to 0.02%.

On the other hand, the influence of the morphological structure is deemed weaker than the influence of the inorganic composition. In a very few cases [60, 61], the structure of char is found to play a more dominant role than the catalytic effect of the ash on char reactivity. For biomass, its char texture and structural organization change over the pyrolysis reaction due to the thermal degradation of the major biomass components, namely, cellulose, hemicellulose, and lignin [62]. Therefore, it seems reasonable the feedstock's lignocellulosic composition content is correlated to the resultant char's reactivity, through influencing the char's textural and structural organization [62], particularly when the feedstock's content of inorganic composition is low and so is its catalytic effect exerted on the char reactivity, as shown in the present study.

4 Conclusion

Feedstock variability is a crucial issue for industrialization of biomass conversion processes. In this research, the CO₂ gasification kinetics of a variety of wood chars, prepared in a high temperature hydrogen flame reactor, was studied in a thermogravimetric analysis by using a non-isothermal method. Three reactivity models were used to calculate the kinetic parameters. In addition, the feedstock effect on the gasification reactivity was also investigated by correlating different biomass property parameters and different reactivity indexes. The following observations were made throughout the study:

- (1) Despite the apparent dependence on the reaction temperature (the T50 and T_{\max} varying from 1018 to 1187 K and from 1029 to 1235 K, respectively), the non-isothermal TG and DTG curves showed strikingly similar qualitative trends for all 40 wood samples. By normalizing the reaction temperature with respect to the T50, the temperature to obtain 50% conversion, the conversion curves can be replotted into one master curve, suggesting that not much variability exists in their reaction mechanism.
- (2) The overall average reaction rates of char gasification (20–95%) vary only modestly (a range from 0.19 to 0.35%/min) when removing the char devolatilization stage from the beginning of the conversion (0–20%). The corresponding feedstock-mean values became progressively higher with the progress of conversion stages. Furthermore, the variation factors also increase for four sequential conversion stages (20–40%, 40–60%, 60–80%, and 80–95%) which indicates the reactivity difference between different feedstock was enlarged.
- (3) All three models (VM, GM, and RPM) predict the gasification conversion profiles relatively well with regression coefficients (R^2) for the predicting conversion curve being all larger than 0.935. The predicted activation energy all falls into a reasonable range, which is consistent with the literature. One other point worth noting is that RPM predicted lower activation energy and it seems to have no advantage over the other two models (VM and GM), which have few unknown kinetic parameters.
- (4) Although the correlation between the reactivity indexes and the fuel characteristic parameters is pretty low, the K content has a relatively strong correlation with R80–95 and R_{\max} . It proved the catalytic effect of potassium functions in the high conversion stages. It seems very challenging to directly relate the biomass characteristics to its gasification performance because of the complexity of these materials and the possible complicated interactions between their properties; however, the present work confirmed the important enhancing role of potassium and found some hints on the positive role of cellulose and negative role of lignin to the char gasification reactivity.

Supplementary Information The online version contains supplementary material available at <https://doi.org/10.1007/s13399-023-04010-5>.

Author contribution Shengyuan Guo: investigation, methodology, and writing – original draft. Zhimin Lu: completing experiments, conceptualization, funding acquisition, supervision, and writing – review and editing. Jinzheng Chen: laboratory analysis, methodology, and writing – review and editing. Zhengyan Bao: writing – review and editing. Jianfeng Cai: writing – review and editing. Shunchun Yao: funding acquisition, resources, and supervision.

Funding This work was supported by the National Natural Science Funds of China (52276190), the Nature Science Foundation of Guangdong Province (2022A1515010741), and the Fundamental Research Funds for the Central Universities (2022ZFH004). We also thank Peter Arendt Jensen, Hao Wu, and Peter Glarborg from DTU CHEC for the help in single particle combustion experiments.

Data availability The datasets used or analyzed during the current study are available from the corresponding author on reasonable request.

Declarations

Ethical approval This article does not contain any studies with human participants or animals performed by any of the authors.

Competing interests The authors declare no competing interests.

References

- IEA (2021) Net zero by 2050: a roadmap for the global energy sector
- National Energy Administration (2021) The National Energy Administration held a press conference to introduce the energy economic situation and other information in the first half of 2021[EB/OL]. http://www.nea.gov.cn/2021-07/29/c_1310093667.htm. Accessed 2021
- China State Forestry and Grassland Administration (2018) Biomass power outlook biomass power share may exceed 5% by 2030 [EB/OL]. <http://www.forestry.gov.cn/zlszz/4264/20181227/160029925465733.html>, 2018-12-27. Accessed 2022
- Shahbaz M, Al-Ansari T, Inayat M et al (2020) A critical review on the influence of process parameters in catalytic co-gasification: current performance and challenges for a future prospectus. *Renew Sustain Energy Rev* 134:110382. <https://doi.org/10.1016/j.rser.2020.110382>
- Trubetskaya A, Timko MT, Umeki K (2020) Prediction of fast pyrolysis products yields using lignocellulosic compounds and ash contents. *Appl Energy* 257:113897. <https://doi.org/10.1016/j.apenergy.2019.113897>
- Di Blasi C (2009) Combustion and gasification rates of lignocellulosic chars. *Prog Energy Combust Sci* 35:121–140. <https://doi.org/10.1016/j.pecs.2008.08.001>
- Sulg M, Konist A, Järvi O (2021) Characterization of different wood species as potential feedstocks for gasification. *Agron Res* 19:276–299. <https://doi.org/10.15159/AR.21.005>
- Dupont C, Nocquet T, Da Costa JA, Verne-Tournon C (2011) Kinetic modelling of steam gasification of various woody biomass chars: influence of inorganic elements. *Bioresour Technol* 102:9743–9748. <https://doi.org/10.1016/j.biortech.2011.07.016>
- Dahou T, Defoort F, Jeguirim M, Dupont C (2020) Towards understanding the role of K during biomass steam gasification. *Fuel* 282:118806. <https://doi.org/10.1016/j.fuel.2020.118806>
- Dupont C, Jacob S, Marrakchy KO et al (2016) How inorganic elements of biomass influence char steam gasification kinetics. *Energy* 109:430–435. <https://doi.org/10.1016/j.energy.2016.04.094>
- Billaud J, Valin S, Peyrot M, Salvador S (2016) Influence of H₂O, CO₂ and O₂ addition on biomass gasification in entrained flow reactor conditions: experiments and modelling. *Fuel* 166:166–178. <https://doi.org/10.1016/j.fuel.2015.10.046>
- Mahinpey N, Gomez A (2016) Review of gasification fundamentals and new findings: reactors, feedstock, and kinetic studies. *Chem Eng Sci* 148:14–31. <https://doi.org/10.1016/j.ces.2016.03.037>
- Nzihou A, Stanmore B, Sharrock P (2013) A review of catalysts for the gasification of biomass char, with some reference to coal. *Energy* 58:305–317. <https://doi.org/10.1016/j.energy.2013.05.057>
- Septien S, EscuderoSanz FJ, Salvador S, Valin S (2018) The effect of pyrolysis heating rate on the steam gasification reactivity of char from woodchips. *Energy* 142:68–78. <https://doi.org/10.1016/j.energy.2017.09.114>
- Wang G, Zhang J, Shao J et al (2016) Experimental and modeling studies on CO₂ gasification of biomass chars. *Energy* 114:143–154. <https://doi.org/10.1016/j.energy.2016.08.002>
- Aranda G, Grootjes AJ, Van Der Meijden CM et al (2016) Conversion of high-ash coal under steam and CO₂ gasification conditions. *Fuel Process Technol* 141:16–30. <https://doi.org/10.1016/j.fuproc.2015.06.006>
- Lu Z, Jian J, Jensen PA et al (2016) Influence of torrefaction on single particle combustion of wood. *Energy Fuels* 30:5772–5778. <https://doi.org/10.1021/acs.energyfuels.6b00806>
- Lu Z, Jian J, Arendt Jensen P et al (2017) Impact of KCl impregnation on single particle combustion of wood and torrefied wood. *Fuel* 206:684–689. <https://doi.org/10.1016/j.fuel.2017.05.082>
- Vassilev SV, Baxter D, Andersen LK, Vassileva CG (2010) An overview of the chemical composition of biomass. *Fuel* 89:913–933. <https://doi.org/10.1016/j.fuel.2011.09.030>
- Goering HK, Van Soest PJ (1970) Forage fiber analyses (Apparatus, Reagents, Procedures, and Some Applications). https://www.researchgate.net/publication/275346632_Forage_Fiber_Analyses_Apparatus_Reagents_Procedures_and_Some_Applications
- Trubetskaya A (2016) Fast pyrolysis of biomass at high temperatures. https://www.researchgate.net/publication/340284598_Fast_pyrolysis_of_biomass_at_high_temperatures
- Li X, Lu Z, Chen J et al (2021) Effect of oxidative torrefaction on high temperature combustion process of wood sphere. *Fuel* 286:119379. <https://doi.org/10.1016/j.fuel.2020.119379>
- Huo W, Zhou Z, Wang F, Yu G (2014) Mechanism analysis and experimental verification of pore diffusion on coke and coal char gasification with CO₂. *Chem Eng J* 244:227–233. <https://doi.org/10.1016/j.cej.2014.01.069>
- Branca C, Di Blasi C (2020) Self-heating effects in the thermogravimetric analysis of wood char oxidation. *Fuel* 276:118012. <https://doi.org/10.1016/j.fuel.2020.118012>
- Branca C, Di Blasi C (2023) Enhancement and inhibition of the oxidation rates of pyrolytic chars from wood loaded with potassium compounds. *Fuel* 331:125886. <https://doi.org/10.1016/j.fuel.2022.125886>
- Sørensen LH, Gjernes E, Jessen T, Fjellerup J (1996) Determination of reactivity parameters of model carbons, cokes and flame-chars. *Fuel* 75:31–38. [https://doi.org/10.1016/0016-2361\(95\)00213-8](https://doi.org/10.1016/0016-2361(95)00213-8)
- Van de Steene L, Tagutchou JP, EscuderoSanz FJ, Salvador S (2011) Gasification of woodchip particles: experimental and numerical study of char-H₂O, char-CO₂, and char-O₂ reactions. *Chem Eng Sci* 66:4499–4509. <https://doi.org/10.1016/j.ces.2011.05.045>
- González-Vázquez MP, García R, Gil MV et al (2018) Unconventional biomass fuels for steam gasification: kinetic analysis and effect of ash composition on reactivity. *Energy* 155:426–437. <https://doi.org/10.1016/j.energy.2018.04.188>
- Wang G, Zhang J, Hou X et al (2015) Study on CO₂ gasification properties and kinetics of biomass chars and anthracite char. *Bioresour Technol* 177:66–73. <https://doi.org/10.1016/j.biortech.2014.11.063>
- Fermoso J, Gil MV, Pevida C et al (2010) Kinetic models comparison for non-isothermal steam gasification of coal-biomass blend chars. *Chem Eng J* 161:276–284. <https://doi.org/10.1016/j.cej.2010.04.055>

31. Ochoa J, Cassanello MC, Bonelli PR, Cukierman AL (2001) CO₂ gasification of Argentinean coal chars: a kinetic characterization. *Fuel Process Technol* 74:161–176. [https://doi.org/10.1016/S0378-3820\(01\)00235-1](https://doi.org/10.1016/S0378-3820(01)00235-1)
32. Momeni M, Yin C, Kær SK et al (2013) Experimental study on effects of particle shape and operating conditions on combustion characteristics of single biomass particles. *Energy Fuel* 27:507–514. <https://doi.org/10.1021/ef301343q>
33. Xu C, Hu S, Xiang J et al (2014) Kinetic models comparison for steam gasification of coal/biomass blend chars. *Bioresour Technol* 171:253–259. <https://doi.org/10.1016/j.biortech.2014.07.099>
34. Kouichi M, Silveston PL (1989) Analysis of gas-solid reactions by use of a temperature-programmed reaction technique. <https://doi.org/10.1021/ef00014a020>
35. Gudka B, Darvell LJ, Jones JM et al (2012) Fuel characteristics of wheat-based dried distillers grains and solubles (DDGS) for thermal conversion in power plants. *Fuel Process Technol* 94:123–130. <https://doi.org/10.1016/j.fuproc.2011.10.019>
36. Branca C, Di Blasi C (2015) Thermogravimetric analysis of the combustion of dry distiller's grains with solubles (DDGS) and pyrolysis char under kinetic control. *Fuel Process Technol* 129:67–74. <https://doi.org/10.1016/j.fuproc.2014.08.019>
37. Branca C, Di Blasi C (2015) A lumped kinetic model for banana peel combustion. *Thermochim Acta* 614:68–75. <https://doi.org/10.1016/j.tca.2015.06.022>
38. Branca C, Di Blasi C (2003) Global kinetics of wood char devolatilization and combustion. *Energy Fuel* 17:1609–1615. <https://doi.org/10.1021/ef030033a>
39. Branca C, Di Blasi C (2021) Burning dynamics of straw chars under the conditions of thermal analysis. *Energy Fuels* 35:12187–12199. <https://doi.org/10.1021/acs.energyfuels.1c01441>
40. Bouraoui Z, Jeguirim M, Guizani C et al (2015) Thermogravimetric study on the influence of structural, textural and chemical properties of biomass chars on CO₂ gasification reactivity. *Energy* 88:703–710. <https://doi.org/10.1016/j.energy.2015.05.100>
41. Alvarez J, Lopez G, Amutio M et al (2019) Evolution of biomass char features and their role in the reactivity during steam gasification in a conical spouted bed reactor. *Energy Convers Manag* 181:214–222. <https://doi.org/10.1016/j.enconman.2018.12.008>
42. Ding S, Kantarelis E, Engvall K (2020) Effects of porous structure development and ash on the steam gasification reactivity of biochar residues from a commercial gasifier at different temperatures. https://www.researchgate.net/publication/344357631_Effects_of_Porous_Structure_Development_and_Ash_on_the_Steam_Gasification_Reactivity_of_Biochar_Residues_from_a_Commercial
43. Bouraoui Z, Dupont C, Jeguirim M et al (2016) CO₂ gasification of woody biomass chars: the influence of K and Si on char reactivity. *Comptes Rendus Chim* 19:457–465. <https://doi.org/10.1016/j.crci.2015.08.012>
44. Gil MV, Riaza J, Álvarez L et al (2012) Oxy-fuel combustion kinetics and morphology of coal chars obtained in N₂ and CO₂ atmospheres in an entrained flow reactor. *Appl Energy* 91:67–74. <https://doi.org/10.1016/j.apenergy.2011.09.017>
45. Seo DK, Lee SK, Kang MW et al (2010) Gasification reactivity of biomass chars with CO₂. *Biomass Bioenergy* 34:1946–1953. <https://doi.org/10.1016/j.biombioe.2010.08.008>
46. Cortazar M, Lopez G, Alvarez J et al (2020) Experimental study and modeling of biomass char gasification kinetics in a novel thermogravimetric flow reactor. *Chem Eng J* 396:125200. <https://doi.org/10.1016/j.cej.2020.125200>
47. Alvarez J, Lopez G, Amutio M et al (2015) Kinetic study of carbon dioxide gasification of rice husk fast pyrolysis char. *Energy Fuel* 29:3198–3207. <https://doi.org/10.1021/acs.energyfuels.5b00318>
48. Gao X, Zhang Y, Li B et al (2016) Determination of the intrinsic reactivities for carbon dioxide gasification of rice husk chars through using random pore model. *Bioresour Technol* 218:1073–1081. <https://doi.org/10.1016/j.biortech.2016.07.057>
49. Sheng XuR, Liang ZJ, Wei WG et al (2016) Gasification behaviors and kinetic study on biomass chars in CO₂ condition. *Chem Eng Res Des* 107:34–42. <https://doi.org/10.1016/j.cherd.2015.10.014>
50. Roncancio R, Gore JP (2021) CO₂ char gasification: a systematic review from 2014 to 2020. *Energy Convers Manag* 10:100060. <https://doi.org/10.1016/j.ecmx.2020.100060>
51. Tanner J, Bhattacharya S (2016) Kinetics of CO₂ and steam gasification of Victorian brown coal chars. *Chem Eng J* 285:331–340. <https://doi.org/10.1016/j.cej.2015.09.106>
52. Gomez A, Silberman R, Mahinpey N (2014) A comprehensive experimental procedure for CO₂ coal gasification: is there really a maximum reaction rate? *Appl Energy* 124:73–81. <https://doi.org/10.1016/j.apenergy.2014.02.077>
53. Gomez A, Mahinpey N (2015) Kinetic study of coal steam and CO₂ gasification: a new method to reduce interparticle diffusion. *Fuel* 148:160–167. <https://doi.org/10.1016/j.fuel.2015.01.071>
54. Silberman R, Gomez A, Gates I, Mahinpey N (2013) Kinetic studies of a novel CO₂ gasification method using coal from deep unmineable seams. *Ind Eng Chem Res* 52:14787–14797. <https://doi.org/10.1021/ie401918e>
55. Struis RPWJ, Von Scala C, Stucki S, Prins R (2002) Gasification reactivity of charcoal with CO₂. Part II: metal catalysis as a function of conversion. *Chem Eng Sci* 57:3593–3602. [https://doi.org/10.1016/S0009-2509\(02\)00255-5](https://doi.org/10.1016/S0009-2509(02)00255-5)
56. Zhang Y, Ashizawa M, Kajitani S, Miura K (2008) Proposal of a semi-empirical kinetic model to reconcile with gasification reactivity profiles of biomass chars. *Fuel* 87:475–481
57. Suzuki T, Nakajima H, Ikenaga N-o et al (2011) Effect of mineral matters in biomass on the gasification rate of their chars. *Biomass Convers Biorefinery* 1:17–28. <https://doi.org/10.1007/s13399-011-0006-2>
58. Struis RPWJ, Von Scala C, Stucki S, Prins R (2002) Gasification reactivity of charcoal with CO₂. Part I: conversion and structural phenomena. *Chem Eng Sci* 57:3581–3592. [https://doi.org/10.1016/S0009-2509\(02\)00254-3](https://doi.org/10.1016/S0009-2509(02)00254-3)
59. Komarova E, Abosteif Z, Guhl S, Meyer B (2019) Brown coal char CO₂-gasification kinetics with respect to the char structure part II: kinetics and correlations. *Can J Chem Eng* 97:226–237. <https://doi.org/10.1002/cjce.23329>
60. Asadullah M, Zhang S, Min Z et al (2010) Effects of biomass char structure on its gasification reactivity. *Bioresour Technol* 101:7935–7943. <https://doi.org/10.1016/j.biortech.2010.05.048>
61. Lv D, Xu M, Liu X et al (2010) Effect of cellulose, lignin, alkali and alkaline earth metallic species on biomass pyrolysis and gasification. *Fuel Process Technol* 91:903–909. <https://doi.org/10.1016/j.fuproc.2009.09.014>
62. Guizani C, Jeguirim M, Valin S et al (2017) Biomass chars: the effects of pyrolysis conditions on their morphology, structure, chemical properties and reactivity. https://www.researchgate.net/publication/317548857_Biomass_Chars_The_Effects_of_Pyrolysis_Conditions_on_Their_Morphology_Structure_Chemical_Properties_and_Reactivity

Publisher's note Springer Nature remains neutral with regard to jurisdictional claims in published maps and institutional affiliations.

Springer Nature or its licensor (e.g. a society or other partner) holds exclusive rights to this article under a publishing agreement with the author(s) or other rightsholder(s); author self-archiving of the accepted manuscript version of this article is solely governed by the terms of such publishing agreement and applicable law.